AIMS Bioengineering

AIMS Bioengineering, 5 (2): 106–132.
DOI: 10.3934/bioeng.2018.2.106
Received: 05 February 2018
Accepted: 10 May 2018
Published: 22 May 2018

http://www.aimspress.com/journal/Bioengineering

Research article

Chemotherapeutic loading via tailoring of drug-carrier interactions in poly (sialic acid) micelles

Gerald Pawlish[1], Kyle Spivack[2], Adam Gabriel[2], Zuyi Huang[2] and Noelle Comolli[2,*]

[1] Department of Bioengineering, College of Engineering, Temple University, 1947 N 12th St, Philadelphia, PA 19122, USA
[2] Department of Chemical Engineering, College of Engineering, Villanova University, 800 E. Lancaster Ave., Villanova, PA 19085, USA

* **Correspondence:** Email: Noelle.Comolli@villanova.edu; Tel: +6105197134.

Abstract: New methods in nanoparticle development have aimed to develop customized carriers suited for specific purposes. Micelles, due to their highly tailorable nature, are prime candidates for this customizable methodology. In order to maximize drug loading and tailor release, groups of the micelle core should be carefully selected in order to exploit inherent interactions between the selected drug and the carrier core. Small variations within the composition of these groups can greatly affect micelle characteristics (e.g., size, stability, loading and release). While covalent bonding of drug-to-carrier has enhanced drug loading, drawbacks include inhibited release and altered drug properties. As a result, drug/carrier non-covalent interactions such as hydrophobic attraction, hydrogen bonding and π-π stacking have all garnered great interest, allowing for both enhanced loading as well as bond dissociation to aid in drug release. Just as important, external composition of these micelles should be suited for specific therapeutic applications. Examples include providing stabilization, enhanced circulation times and site-specific targeting. Poly (sialic acid) (PSA), a naturally occurring polysaccharide, has been shown to exhibit all three of these properties yet remains relatively unexplored in the field of micelle-based cancer drug delivery applications. Here, we have grafted various phenyl-terminated alkyl groups (PTAGs) onto the backbone of PSA (PTAG-*g*-PSA), each selected in order to exploit a specific non-covalent interaction (hydrophobic attraction, hydrogen bonding and π-π stacking) between the PTAG group and the anthracycline chemotherapeutic doxorubicin (DOX) (Figure 1). Upon aqueous self-assembly, these amphiphiles formed micelles which exhibited variation in size, stability, cytotoxicity and DOX loading/release based upon the PTAG selected. For example, PTAGs selected to exploit either hydrogen bonding or π-π stacking loaded in a similar fashion yet varied greatly in release properties.

Therefore, the synergistic effect of these small-scale modifications in core groups selected can greatly effect micelle characteristics and result in highly tailorable carriers.

Keywords: cancer; hydrogen bonding; micelles; nanomedicine; non-covalent bonding; pi-pi stacking; poly (sialic acid)

1. Introduction

Within the next 15 years, the number of deaths attributed to cancer are expected to nearly double, expanding from 7.6 million to 13.1 million [1]. While the long established standard treatment of care, chemotherapy is prone to limited tumor specificity and restricted antitumor activity [2]. This lack of tumor targeting can result in systemic toxicity, thereby limiting the dosage needed for effective tumor treatment. Many of these chemotherapy agents are highly hydrophobic in nature (e.g., paclitaxel, docetaxel and cabaziaxel), greatly contrasting the aqueous environment encountered upon administration and impeding long-circulation times [3].

The chemotherapeutic doxorubicin (DOX) is used in a wide array of cancers including hematological malignancies, carcinomas and soft-tissue sarcomas [4]. The presence of anthracene rings within the molecular structure of DOX imbues its strong hydrophobicity, thereby allowing for passive diffusion through the cellular phospholipid bilayer [5]. Once inside, intracellular complexation with DNA and/or covalent binding to other proteins associated with replication and transcription result in cellular death [6,7]. While effective, significant side effects of DOX include myelosuppression, cardiotoxicity, nausea, diarrhea, loss of hair, ulcers and necrosis [8]. These side effects arise from accumulation of DOX at non-targeted tissue resulting from drug overflow from the blood vessels [2,4]. The salt form of DOX (DOX-HCl), while exhibiting high aqueous solubility (10 mg/mL) [5], can result in accumulation and damage at off-target sites such as the heart, liver and lung [8]. This has lead to the need to not just reformulate DOX, but many other chemotherapeutics in order to enhance their therapeutic index [4].

In order to accomplish this, new and innovative approaches towards the delivery of these chemotherapeutics are being formulated. A great deal of interest lies within the use of nanotechnology to accomplish this, especially within the field of nanomedicine [9]. A large segment of this field of study aims to selectively target chemotherapeutics towards tumor sites, control their delivery upon arrival, increase drug efficacy, bioavailability and ultimately their therapeutic effect [1], greatly contrasting the non-specific approach of many clinically used cancer agents. Polymeric micelles have long been viewed as a proper platform to accomplish this [10–14]. Formed from the self-assembly of amphiphilic block or graft copolymers, polymeric micelles are colloidal particles 10–200 nm in size containing a hydrophobic core and hydrophilic shell [15]. Micelles have the ability to load chemotherapeutics, such as DOX, within their hydrophobic core and thereby sufficiently increase drug solubility, stability, circulation time and tumor-specific targeting [12]. In contrast, freely administered drugs tend to exhibit difficulty in penetration and distribution within the tumor site due to dependence on convection/diffusion within the tumor interstitium, ultimately resulting in low therapeutic efficacy [8]. Drug-loaded nanoparticles (e.g., micelles) can take advantage of discrepancies between tumor and normal tissue to offset this issue. Tumor characteristics such as hypervascularity, incomplete vascular architecture, vascular permeability

factor secretion, compromised lymphatic drainage and high interstitial pressure can lead to micelle extravasation within the tumor [16]. This phenomena, known as the Enhanced Permeation and Retention (EPR) effect, can greatly increase micelle buildup and particle residence times within the tumor, thereby aiding in enhanced drug buildup.

While promising, many of these micelle-based drug carriers exhibit poor core stability and premature drug leakage upon *in-vivo* administration [4]. This leads towards unnecessarily higher dosages to reach the full therapeutic effect, potentially incr easing the risk of toxicity [3]. Methods of enhancing core stability have varied. Covalent cross-linking of the core, shell or interface have augmented circulation times yet resulted in poor drug retention, premature release and extraction of the drug *in-vivo* [17]. Loading capacity (LC) and encapsulation efficiency (EE) of micelles can range greatly based upon drug loading methods used, loading space within the drug carrier, core crystallinity and carrier glass transition temperature thereby making the prospect of a "one-size-fits-all" carrier unlikely [3]. In turn, tailoring the carrier to fully exploit the properties of the drug has been proposed as the next logical step [15], prompting the idea to find a match between the drug and core forming section of the micelle to boost loading and maintain stability [18]. While chemical conjugation of the drug to the carrier has in fact significantly enhanced circulatory stability, drawbacks have included significant alteration of parent drug biological properties, slow drug release and diminished therapeutic effect [3,17].

In contrast, non-covalent drug/carrier interactions such as hydrogen bonding, electrostatic/hydrophobic interactions, and π-π stacking have all been viewed with great interest [3]. Of these, π-π stacking has garnered particular attention in micelle drug delivery systems [17,19–22]. π-π interactions involve the non-covalent attractions which occur between different aromatic rings, naturally found within nucleobase stacking, structural folding of proteins and molecular recognition [3]. π-π stacking is partially directional in nature, arising in T-shaped, sandwich or parallel displacement ring conformations resulting from the formation of weak three-dimensional "structures" [3]. The use of π-π stacking, while relatively low in strength (8–9 kJ/mol) [3], can still improve the encapsulation properties and stability of micelle carriers loading drugs containing aromatics (e.g., chemotherapeutics). The addition of aromatic groups along the internal polymer backbone can result in π-π stacking with aromatic-containing chemotherapy drugs upon micelle loading [17]. This has been exhibited numerous times in examples such as paclitaxel [15,16], docetaxel [18] and DOX [5,23,24]. Micelles developed by Shi et al. [17] containing aromatic rings within the hydrophobic block loaded up to 34 wt.% of docetaxel, resulting in one of the highest loadings for micelles ranging between 60–80 nm, and released 50% less PTX after 10 days than micelles without aromatic modification. The use of π-π stacking via pedant benzyl residues within the micelle core has also been exploited by Kataoka et al. [20] to load DOX within poly(ethylene glycol)-poly(β-benzyl-L-aspartate) micelles, resulting in high drug loading (15–20 wt.%) and micelle core stabilization. It has been proposed significant modification of the copolymer is not needed, as the addition of just one aromatic group within the backbone has been shown to increase loading within micelles [3].

While the properties of many of these micelles were improved via π-π stacking, loading and stability were further enhanced through the addition of other non-covalent (hydrophobic attraction, hydrogen bonding) forces working in tandem to provide multiple non-covalent intermolecular forces between drug and carrier [15,16,20,23,24]. DOX contains a significant number of hydrogen bond donors (e.g., hydroxyls, primary amines), indicating that a carrier containing hydrogen bond

acceptors (e.g., ethers, carbonyls) within its core could be beneficial towards drug loading [24]. Benefits of having these groups within the core-forming section of the micelle stem from lack of competition with water for hydrogen bonding sites, such as would be found in the surrounding polar environment [3]. Hydrogen bonds within polar environments are known to be significantly weaker than those which exist explicitly in non-polar environments due to this competition [3]. This can make drug/carrier hydrogen bonding within the micelle core of sufficient strength to enhance loading. Thereby, it is largely indicative that a synergistic approach can be highly beneficial towards fully realizing the maximum loading potential of many chemotherapeutics. The micelle should be tailored to suit the properties of the drug, in essence creating a "match" between the drug and micelle core forming sections.

While the core-forming hydrophobic segment of the micelle will largely dictate how the drug is loaded within the micelle, the ultimate destination of the carrier is predicated upon its interaction with the aqueous environment and tissue vasculature once in circulation. This interaction is largely governed by the hydrophilic component of the micelle, making its selection just as important as the core-forming segment. These groups which are selected are normally high molecular weight and weakly anionic macromolecules, providing a protective shield around the micelle [25]. Hydrophilic polymers such as these can effectively repel opsonin proteins which would normally mark the micelle for premature clearance by the immune system. This, thereby, provides the carrier a stealth-like element and increases particle circulation times via reticuloendothelial system (RES) evasion [1].

Of these stealth-coatings, the synthetic polymer poly (ethylene glycol) (PEG) has long become the gold standard of hydrophilic coatings given its high biocompatibility and non-toxic nature [26]. PEG's sufficient hydrophilicity allows for each repeating unit to hydrogen bond with three water molecules [27], thus forming a protective "watery cloud" [28] around PEGylated particles from immune system detection. While PEG-based coatings have become commonplace in drug delivery systems [29], an underlying "PEG Problem" [25] has recently arisen. Limited interaction with cells [30], rapid excretion by the kidneys [28], induction of antiPEG-IgM in both humans and animals [31], intracellular buildup due to poor degradation properties and potential toxicity associated with PEG-oxidation [25] have all been associated with PEG-based delivery systems. As a result, a number of hydrophilic surface coatings are being explored as alternatives to PEG [32]. Polysaccharide-based systems [33], based upon their similar hydrophilic properties to PEG, have been viewed as such. While PEG hydrogen-bonds with three water molecules per repeat unit, polysaccharides can associate with as many as four to six per repeat unit [27], thereby providing the same protective "watery cloud" as exhibited by PEG.

Of these potential polysaccharide-based coatings, poly (sialic acid) (PSA) has garnered a great amount of interest [25,27,34,35]. PSA, a polysaccharide-based homopolymer of sialic acid in either α-2,8 or α-2,9 linkages, is non-immunogenic and biodegradable [30]. Considerably anionic, PSA is highly expressed on red blood cells and metastatic cancer cells as well as formed on the surface of invading pathogens [30], leading to the long circulation times and immune system evasion associated with these. PSA has been viewed as the human body's natural form of a "stealth" coating. Surface expression of *N*-acteylneuraminic acid [2] by eukaryotic cells results in the inhibition of self-tissue by low-level alternative complement activation [1], thereby allowing for long cell circulation times. While expression of PSA by erythrocytes allows for residence times of nearly 120 days within circulation, sialidase treated cells were shown to decrease circulation times from nearly 4 months to only a few hours within humans [35,36]. This indicates the significant importance of PSA in cellular

circulation and lifetime. PSA is also commonly expressed on the surface of pathogenic bacteria [37], allowing for *Neisseria Meningitides* and *Pasteurella haemolytica* to avoid detection by the immune system though use of a PSA "mask" [27]. These naturally occurring examples have made PSA of significant relevance for the development of long-circulating drug delivery systems. Along with the addition of long-circulating properties, PSA also has been of great interest in cancer applications. These have included tumor targeting [30,38,39], enhancing uptake in cancer cell populations [2,40,41], as well as inhibition of metastatic tumor growth [42]. PSA-based systems, while not as prevalent as PEG, have been effective. Small molecule [28], pro-drug [2] and nanoparticle [35,40,43] modifications have been formulated, yet an untapped interest lies in addition of PSA to micelle-based systems [25,27,34,44] with specific use in cancer applications.

In this study, we have developed micelles composed of various phenyl-terminated alkyl groups (PTAG's) grafted onto PSA (PTAG-*g*-PSA). Through this, we sought the optimal characteristics for loading and release of DOX through small variations within the PTAG core forming segments. These included changes in alkyl chain length (PEA, PPA, PBA), polarity (POE) as well as additional sites for π-π stacking via additional phenyl groups (33DPP). The compositions of these micelles were synergistically tailored to load DOX via a multitude of hydrophobic interactions (alkyl chain segment), hydrogen bonding (ester/ether groups) and π-π stacking (terminal phenyl groups) based upon the PTAG group selected.

2. Materials and methods

2.1. Materials

Chemicals and solvents of analytical grade were purchased and used as received. Fetal Bovine Serum (FBS) was purchased from Atlanta Biologicals. Colominic acid sodium salt (PSA, 30 kDa isolated from *E. coli*) was obtained from Nacalai USA as well as Carbosynth. Dimethylsulfoxide (DMSO) was obtained from Fisherbrand. Dulbecco's Modified Eagle Medium (4.5 g/L *D*-Glucose, *L*-Glutamine) (DMEM), Phosphate Buffered Saline (pH 7.4, Without Calcium/Magnesium/Phenol Red) (PBS), Penicillin-Streptomycin (Pen Strep) and Trypsin-EDTA (0.25%, phenol red) were purchased from Gibco. Vybrant™ MTT (3-(4,5-Dimethylthiazol-2-yl)-2,5-Diphenyltetrazolium Bromide) Cell Proliferation Assay Kit was obtained from Invitrogen. *N*-(3-Dimethyl-amino propyl)-*N'*-ethylcarbodiimde (EDC), *N*-hydroxysuccinimide (NHS), Deuterium oxide (D, 99.9%; 0.05 wt.% TMS) (D_2O), Phosphate Buffered Saline 1× (PBS), Phenylethylamine (PEA), 2-Phenoxyethylamine (POE), 3-Phenyl-1-propylamine (PPA), 3,3-Diphenylpropylamine (33DPP), 4-Phentylbutylamine (PBA), and Triethylamine (TEA) were purchased from Sigma-Aldrich (St. Louis, MO) and used as received. 0.45 μm PVDF-L Filters (13 mm diameter) were purchased from Simsii. Snakeskin MWCO 3.5 kDa Dialysis Tubing, Dulbecco's Modified Eagle Medium (DMEM) and Hank's Balanced Salt Solution (HBSS) were purchased from Thermo Scientific. Doxorubicin (Hydrochloride Salt, >99%) was purchased from LC Labs and used as received. LCB3 human glioblastoma cells were obtained as a gift from Dr. Cezary Marcinkiewicz of Temple University.

2.2. Synthesis of PSA amphiphiles

The synthesis of PSA amphiphiles (Figure 1) was performed in a similar fashion as described by

Bader et al. [25]. In short, PSA was dissolved in DD_2O so as reach a concentration of 6 mg/mL. The carboxylic acid groups of the PSA were then activated through the addition of EDC and NHS and allowed to mix for 30 minutes at room temperature. The selected phenyl-terminated alkyl group (*PTAG*; PEA, PPA, PBA, POE or 33DPP) was then added and allowed to react overnight. The addition of EDC, NHS and respective PTAG were all added in equimolar ratios to a constant PSA backbone in order to obtain 50–60% Degree of Substitution (DOS) of the carboxylic acids along the PSA. In cases of varied DOS formulations for 33DPP-*g*-PSA and POE-*g*-PSA, the values were adjusted to result in 20–30% and 90–100% DOS respectively. The product was then filtered through a 0.45 μm PVDF filter, dialyzed against water for 24 h (MWCO = 3.5 kDa, water change twice at 4 h/18h), filtered again, frozen at −80 ℃ and lyophilized.

2.3. ^{1}H-NMR spectroscopy

3 mg of lyophilized PTAG-*g*-PSA was dried in a desiccator for 48 hours to remove residual water from the sample. Once complete, the resulting product was resuspended in 1 mL of D_2O (0.05 wt.% TMS) and analyzed using a Brunker 500 NMR instrument.

2.4. Size, dispersity and zeta (ζ)-potential measurements of micelles

Lyophilized, dried micelles were resuspended in DD_2O so as to yield the required concentration. These were filtered through a 0.45 μm PVDF filter to remove potential aggregates. Both unloaded and DOX-loaded micelles were treated in the same fashion. Size and PDI measurements were performed at 25 ℃ using a Brookhaven sizing instrument (scattering angle 90 °, wavelength 657 nm). ζ_{POT} of the micelles were evaluated in a similar fashion but were assessed through the use of a Malvern Zetasizer Nano ZS.

Dilution studies were performed in a similar fashion, with the maximum concentration continually diluted with DD_2O until all the required concentrations were reached. Micelles were allowed to sit for 10 minutes between each dilution to reach stability with no additional filtration required. The same sample was used to ensure comparative results.

2.5. Scanning electron microscopy (SEM)

The size and morphological properties of micelles were assessed through the use of a Hitachi S-4800 Scanning Electron Microscope. 200 μL of the micelle suspension at 1 mg/mL in DD_2O were plated on a carbon tape and allowed to dry overnight in a vacuum desiccator. Upon drying, the particles were sputter coated with gold and visualized through the use of a SEM at 10 kV. The micelles were diluted so only one particle would be within the field of view.

2.6. Micelle loading and release

2.6.1. Micelle loading

Micelle loading was performed by a commonly established dialysis method [11]. DOX loading was evaluated so as to yield either 5, 10 or 15 wt./wt.% DOX to PTAG-*g*-PSA. In brief, 1 mg of

DOX-HCl (e.g., 10 wt./wt.%) and 10 mg of PTAG-*g*-PSA were dissolved in 1 mL DMSO and vortexed at 3000 rpm for 1 minute. 5 μL of TEA was added to remove the HCl from DOX, thereby resulting in free DOX in its purely hydrophobic form. This solution was mixed at 300 rpm for 2 h at room temperature and added in a drop-wise fashion to 5 mL DD_2O using a 21 g needle to initiate micelle formation. After mixing for 5 minutes at 300 rpm, the resulting micelle suspension was quickly transferred to a pre-swollen dialysis bag (MWCO 3.5 kDa). The DOX-loaded micelles were then dialyzed against DD_2O for 24 hours (300× dialysate volume) to remove unloaded DOX, TEA-HCl, and TEA. Four dialysate changes performed over the dialysis period. The product was then filtered through a 0.45 μm PVDF to remove unloaded DOX and DOX-PSA aggregates, frozen at −80 ℃ and lyophilized until a dry product was obtained. These were stored dry at 4 ℃ until further use. Loading Capacity (LC; Eq 1) and Encapsulation Efficiency (EE; Eq 2) were determined via dissolution of DOX-loaded micelles in DMSO and assessing absorbance at 485 nm via a DOX calibration method.

2.6.2. Micelle release

DOX release from select drug loaded PTAG-*g*-PSA micelles was performed so as to assimilate response at physiological conditions and intracellular conditions upon systemic administration. To accomplish this both PBS (10 mM, pH 7.4) and sodium acetate buffer (10 mM, pH 5.0) were used. Before addition of the micelles to the dialysate, 1/4 of the buffer volume was removed, set aside and replaced with fresh buffer. Based upon results from loading assays, DOX-loaded micelles equivalent to 350 μg/mL of DOX were resuspended in the respective buffer at 37 ℃ and immediately transferred into a pre-swollen dialysis bag (MWCO 3.5 kDa). The micelles were then placed on dialysis at 37 ℃ with stirring (100 RPM) with 10× volume dialysate buffer-to-suspension. 1/4 of the buffer volume was removed at predetermined time points. To assess DOX release, collected samples at the various time points were assessed through absorption at 485 nm and evaluated via a DOX calibration curve.

2.6.3. Modeling micelle release

In order to quantitatively monitor the drug burst phase and effective drug diffusivity that cannot be directly determined from the release profiles by eye inspection, the release data was also fit to a model shown in Eq 3 that was previously described in Donaldson et al. [51], to quantify the drug release dynamics for the micelles developed in this work. The first segment of Equation 3 deals with the burst phase and the second segment deals with the diffusional phase. The detail of the parameter estimation has been previously published in Donaldson et al.

2.7. Cytotoxicity

LBC3 human glioblastoma cells were seeded on plasma treated 96-well tissue culture plates at 10,000 cells/well and incubated overnight at 37 ℃/5% CO_2. 1 hour before particle introduction the following day, 150 μL of fresh media was added to the plate. In order to obtain proper micelle concentrations within each well, micelle suspensions in PBS (10 mM, pH 7.4) of each PTAG-*g*-PSA formulation were made at 4× the assayed concentration. These suspensions were then filtered

through 0.45 μm PVDF filters and 50 μL of each suspension was added to their respective wells. The remaining suspension were serially diluted with PBS and added to the plate in the same fashion. This resulted in final concentrations within the wells ranging from 7.9–1000 μg/mL. Control cell populations were administered PBS. The plate was then incubated (37 ℃/5% CO_2) for 48 hours. Upon completion of incubation, the media was removed and the wells were washed thrice with warm PBS with a final addition of 100 μL new fresh media. To this, 10 μL of MTT reagent (5 mg/mL in 1 × PBS) was added to each well and the plate was incubated for another 4 h. In order to stop the reaction, the MTT/DMEM was removed from each well and replaced with 200 μL of DMSO. The formazan produced by live-cells was dissolved through multiple triturations and the plate was measured at 590 nm via the use of a BioTek Synergy HT Microplate Reader plate reader. Cell viability (%) was assessed through comparing the absorbance values of treated micelle populations to the absorbance of untreated PBS-control wells.

2.8. Cell culture

LBC3 human glioblastoma cells were grown on 75 cm^2 tissue culture flasks in DMEM with 10% FBS, 4.5 g/L glucose, 4 mM L-glutamine, 1% non-essential amino acids, 100 U/mL penicillin and 100 μg/mL streptomycin. Cells were kept at 37 ℃ in a humidified incubator with 5% CO_2.

2.9. Statistical analysis

All experiments were carried out independently and in triplicate with data presented as mean ± SD. Data was analyzed through the use of JMP Statistical Analysis Software and expressed as the mean ± standard deviation of three independent experiments. Quantitative comparison between two specific groups was performed through the use an F-Test followed by a Student's *t* test assuming equal or unequal variance. A one-way ANOVA was used in instances where more than 3 groups were compared with individual p-values obtained via the use of a post-hoc Tukey HSD test. Significance thresholds of obtained p-values were set as follows. * $p < 0.05$; ** $p < 0.01$; *** $p < 0.001$; **** $p < 0.0001$; n.s. no significance. In table form, the following notation was used to designate such significance: $^{\#}$ $p < 0.05$; $^{\wedge}$ $p < 0.01$; * $p < 0.001$; Δ $p < 0.0001$; ^{x} no significance.

3. Results

PSA grafted with various Phenyl Terminated Alkyl Groups (PTAG's) was synthesized via EDC/NHS chemistry (Figure 1) through modification of a protocol established by Bader et al. [25].

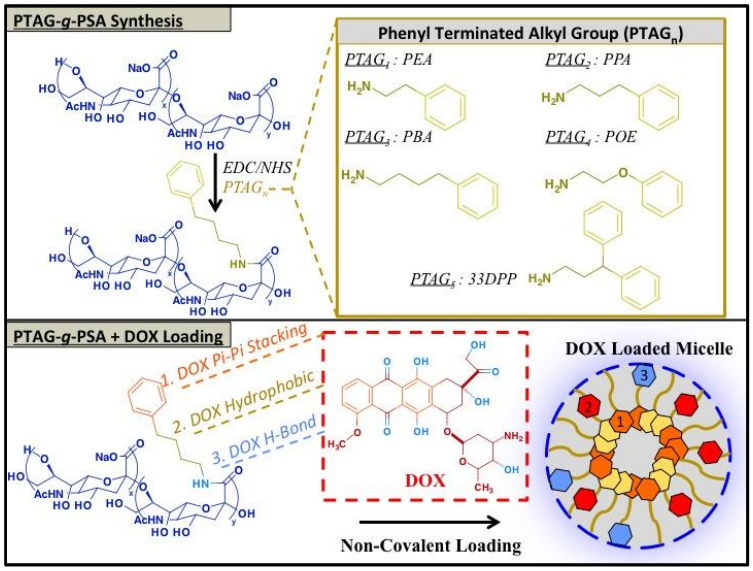

Figure 1. The formation of PTAG-*g*-PSA via EDC/NHS chemistry creates a tailored drug delivery vehicle for chemotherapeutic delivery. The addition of phenyl terminated alkyl group's (PTAG's) on the backbone of PSA allowed for non-covalent (π-π stacking, hydrophobic attraction, hydrogen bonding) interactions with the chemotherapeutic Doxorubicin (DOX), providing a drug delivery vehicle tailored towards exploiting the properties of the drug to enhance loading. Activation of the carboxylate group of PSA via EDC/NHS chemistry allowed for carbodiimide coupling with PTAG's containing terminal amine groups, resulting in the formation of PTAG-*g*-PSA. Initial molar feed rates of each PTAG were kept constant so as to yield a theoretical 20–30%, 50–60%, or 90–100% Degree of Substitution (DOS) along the PSA backbone.

In order to determine the actual extent of modification by the PTAG group on the PSA as a result of the EDC/NHS reaction, ^{1}H-NMR (300 Mz, D_2O, δ ppm) was used (Figure 2).

All peaks were normalized via TMS at 0 ppm. The main structural peaks of PSA were assessed (Table S1) followed by PSA modification from the EDC/NHS reaction (Table S2). Similar to those obtained by Bader et al. [25], PSA monomers were found to be modified with a *N*-acylurea side product due to a rearrangement of the *O*-acylisourea intermediate. As a result of the EDC/NHS carbodiimide coupling step between the PSA and PTAG, the final PTAG-*g*-PSA product contained an amide bond near 3.0 δ. This was used to confirm coupling of the selected PTAG group to the PSA. For ease of interpretation, the peak assignments from the terminal phenyl group were designated as either *ortho*, *meta* or *para* orientations (Table S3).

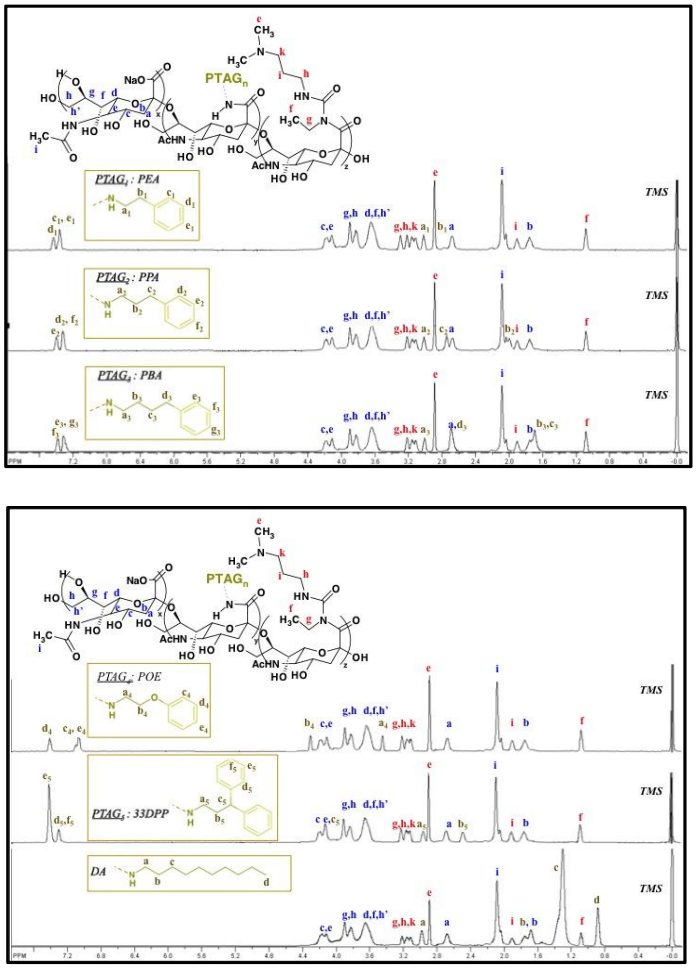

Figure 2. ^{1}H-NMR spectra of PTAG-*g*-PSA formulations with 50–60% DOS. Degree of Substitution (DOS) was determined via comparison of the acetyl (-$NHCOCH_3$, δ 2.1 ppm) peak of PSA with the phenyl (C_6H_5, δ ~7.0–7.4 ppm) peak of each respective PTAG group.

All of the PTAG-*g*-PSA groups exhibited the required amide bond at 3.0 δ with the exception of POE-*g*-PSA. The presence of the ether group within the chain enhances the electronegativity of POE-*g*-PSA and shifted the amide peak from 3.0 δ to 3.4 δ. Actual DOS was determined through the comparison of distinguishing peaks between the PSA backbone and the grafted PTAG moiety (Table 1). In this case, the acetyl (-$NHCOCH_3$, 2.1 δ) and phenyl (C_6H_5, 7.0–7.4 δ) groups were chosen for PSA and each PTAG group respectively. Integrated peaks areas at δ 7.0–7.4 ppm/δ 2.1 ppm were compared for acetyl and phenyl groups for each formulation, yielding consistently 50–60% DOS at 50–60% feed rates. While *N*-acylurea was present along the PSA backbone due to resulting side product formation during the EDC/NHS reaction, this has not been noted to have any significant cytotoxic effect on cells [25,47].

Table 1. Characterization of PTAG-*g*-PSA micelles varied with changes in internal composition size, dispersity and stability varied based upon small variations within the hydrophobic PTAG group. DOS of PTAG-*g*-PSA formulations 50–60%.

PTAG-g-PSA	PTAG DOS (mol %)		Size (nm)[b,d]	PDI[b,d]	ζ_{Pot} (mv)[b,e]
	Feed[a]	Product[c]			
PEA-*g*-PSA	60	55.1	190 ± 26	0.35 ± 0.02	−30 ± 1
PPA-*g*-PSA	60	52.1	166 ± 15	0.38 ± 0.02	−28 ± 2
PBA-*g*-PSA	60	55.7	161 ± 15	0.37 ± 0.05	−33 ± 2
POE-*g*-PSA	60	54.9	194 ± 69	0.32 ± 0.01	−22 ± 2
33DPP-*g*-PSA	60	54.1	133 ± 11	0.35 ± 0.03	−37 ± 5

[a]: PTAG/PSA (mol./mol.); [b]: Mean ± SD (n = 3); [c]: Determined by ^{1}H NMR (D_2O as solvent); [d]: Determined by DLS; [e]: Determined by Malvern Zetasizer Nano ZS.

All PTAG-*g*-PSA groups were resuspended at aqueous conditions from their dry, lyophilized state and evaluated for variations in size and dispersity (Table 1). Properties were shown to vary based upon making slight changes to the composition of the PTAG group. Upon resuspension in water, these PTAG-*g*-PSA amphiphiles self-assembled into polymeric micelles ranging in sizes from 130–190 nm (PDI; 0.32–0.38). The use of SEM confirmed the formation of spherical, round micelles (Figure 3).

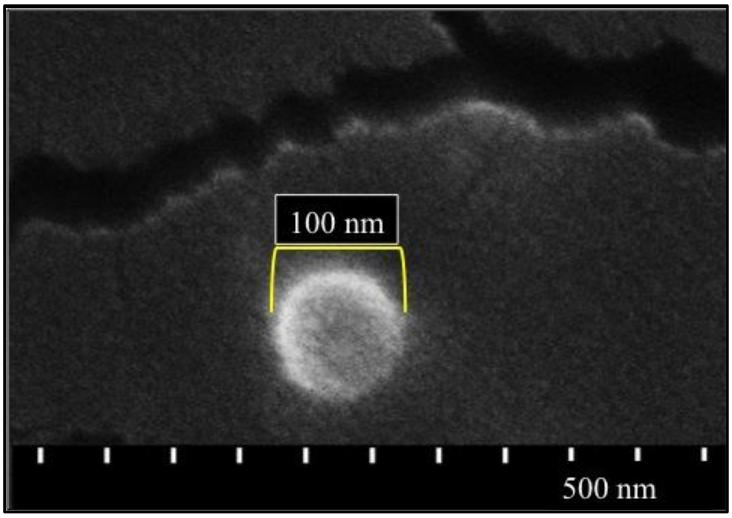

Figure 3. PBA-*g*-PSA self-assembled into spherical micelles under aqueous conditions. Differences between sizes of "wet" (DLS) and "dry" (SEM) formulations resulted from the dehydration of the large hydration layer of PSA. Samples were diluted such that only one micelle was visible within the viewing area. The image scale is in total 500 nm with 50 nm increments. DOS of PTAG-*g*-PSA formulations 50–60%.

Discrepancies between SEM and DLS analysis were believed to be a result of the presence of a hydration layer when analyzed as aqueous suspensions. Due to their distinct interaction with water [35], carriers with hydrophilic coatings have been shown to exhibit larger diameters in their hydrated state (DLS analysis) as compared to their air-dried/dehydrated state (SEM analysis) [15]. These micelles also exhibit a well-defined corona, an indication that the micelles are tightly

packaged [46]. Decreases in micelle sizes with overall increases in PTAG hydrophobicity can be assumed to be a result of the formation of better-defined hydrophobic cores resulting from enhanced inter-polymer hydrophobic interactions between longer chains of opposing amphiphiles during micelle formation. This was reaffirmed from ζ_{POT} values, an indicator of the colloidal stability of the system. Varying from −22 to −37 mV depending upon the PTAG group used, longer or more hydrophobic chains resulted in better colloidal stability.

Encapsulation of DOX within the micelles was performed by first maintaining a constant feed rate of 10 wt./wt.% DOX/Polymer via the dialysis method and evaluating micelle characteristics (Table 2).

Table 2. Addition of Doxorubicin (DOX) increased size and stability of PTAG-*g*-PSA micelles via hydrophobic core stabilization. Loading Capacity (LC) and Encapsulation Efficiency (EE) were enhanced with increasing alkyl chain length, hydrogen bonding or π-π stacking sites within the PTAG chain. DOS of PTAG-*g*-PSA formulations 50–60%.

PTAG-g-PSA	DOX Loading		Size + DOX (nm)[a,c]	PDI + DOX[a,c]	ζ_{Pot} (mv)[a,d]
	LC (%)[b]	*EE (%)*[b]			
PEA-*g*-PSA	2.7	13.5	226 ± 15[#]	0.29 ± 0.02[#]	−38 ± 3[^]
PPA-*g*-PSA	3.0	16.3	204 ± 7[#]	0.26 ± 0.02[^]	−35 ± 1[#]
PBA-*g*-PSA	3.1	19.3	195 ± 16[#]	0.17 ± 0.01[^]	−29 ± 1[#]
POE-*g*-PSA	2.9	16.9	209 ± 16[x]	0.14 ± 0.01[Δ]	−34 ± 1[*]
33DPP-*g*-PSA	3.6	24.0	168 ± 5[^]	0.21 ± 0.01[*]	−37 ± 2[x]

[a]: Mean ± SD (n = 3); [b]: Feed ratio of DOX to polymers was 10 wt./wt.%; [c]: Determined by DLS; [d]: Determined by Malvern Zetasizer Nano ZS.

Loading Capacity (LC; 2.7–3.6%) and Encapsulation Efficiency (EE; 13.5–24.0%) values were enhanced upon increasing alkyl chain length (PEA, PPA, PBA) or the number of hydrogen bonding (POE)/π-π stacking (33DPP) sites within the PTAG group. Interestingly, all properties of the DOX-loaded micelles were significantly enhanced over their unloaded counterparts. As a result of DOX present within the core of the micelle, the micelle size increased close to 20% over nearly all formulations in their unloaded state. In turn, PDI and ζ_{POT} values indicated an increase in overall micelle stability again correlated to the composition of the PTAG chain. Change in PDI was greatest in PTAG formulations where there was the enhanced potential for DOX/Polymer interactions either by increasing alkyl chain length (PEA-PPA-PBA transition), hydrophobicity/π-π stacking sites (33DPP) or chain polarity/hydrogen bonding sites (POE). This correlated back to the enhancements found in LC and EE upon the evaluation of each group.

While overall loading enhancements are key in micelle design, the development of a cytotoxic carrier can effectively nullify any improvements made. In order to evaluate this, unloaded micelles were introduced to LBC3 cells (Figure 4).

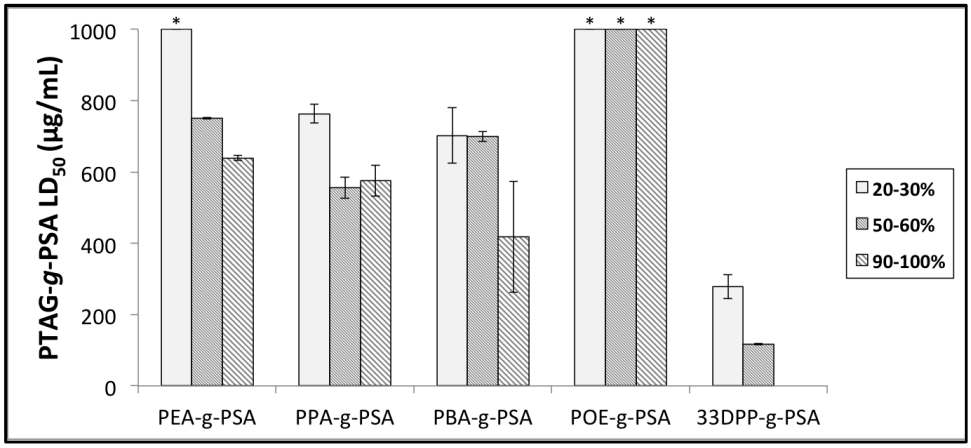

Figure 4. LD_{50} Values of PTAG-*g*-PSA micelles towards LBC3 GMB cell type were proportional to PTAG alkyl chain length and composition. Cell toxicity increased with higher DOS of each PTAG group (20–30%, 50–60%, 90–100%). Decreasing the alkyl chain length or enhancing the polarity of the PTAG group effectively decreased the cytotoxic response. The use of * designates LD_{50} values greater than the assayed amounts.

Increasing the alkyl chain length from (PEA/PPA/PBA) initiated a cytotoxic response within the assessed LBC3 populations. 33DPP-*g*-PSA continued this trend, as the addition of the pendent phenyl group greatly reduced biocompatibility with the cells. In contrast, the additional polar group of POE-*g*-PSA enhanced IC_{50} values to greater than 1000 µg/mL. At this point, it was determined that 33DPP-*g*-PSA, while maintaining the best loading results, would be used exclusively for micelle characterization studies while POE-*g*-PSA, given its sufficiently low cytotoxicity, would be suitable for both characterization and *in-vitro* studies. Both of these formulations were varied in initial PTAG feed, thereby varying the final DOS, and loaded with 10% DOX (Figure 5).

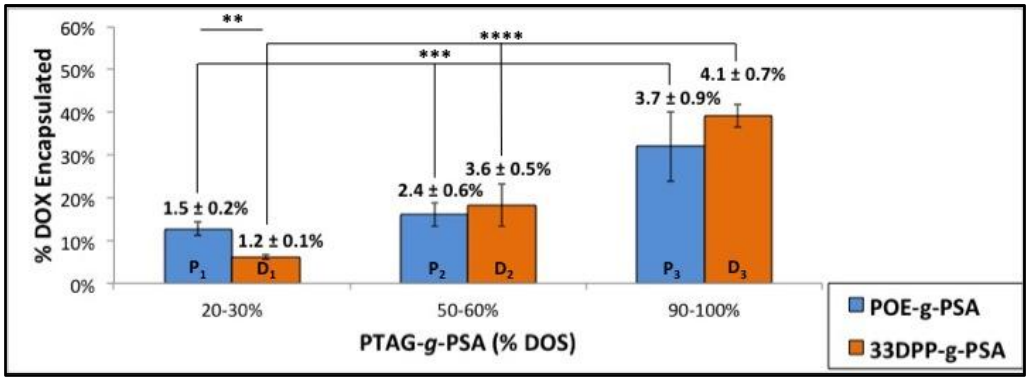

Figure 5. Enhancement in DOX loading was obtained by increasing the DOS of the selected PTAG group. Enhancing DOS (20–30%, 50–60%, 90–100%) along the PSA backbone resulted in more drug-polymer interaction sites and thereby greater drug loading. Loading capacity listed above error bars. P and D values within graphs designate post-hoc Tukey HSD test (see Supplemental materials).

As the DOS of the selected PTAG group increased along the backbone from 20–30%, 50–60% and 90–100%, there was a significant increase in DOX loading in both POE-*g*-PSA and 33DPP-*g*-PSA formulations respectively. This is consistent with the idea that additional hydrophobic chains within the micelle aid in drug loading enhancements. While no difference observed at 50–60% substitution between POE and 33DPP, variations between formulations were noted at low substitution (20–30%) and highly substituted (90–100%). The EE of POE formulations at 20–30% DOS was nearly double that compared to 33DPP formulations at the same DOS. In contrast, high substitution at 90–100% resulted in 33DPP groups exhibiting both higher average values and less deviation between those obtained. 90–100% groups were then used in subsequent experiments due to their high loading values. As noted previously, micelle PDI's all dropped drastically over their unloaded equivalents yet sizes of both 20–30% and 50–60% were larger than their unloaded counterparts while 90–100% were smaller, indicating a potential change in micelle formation upon higher DOS (see Supplemental materials).

Next, the exact drug feed needed to exploit maximal DOX loading was determined. To accomplish this, both POE-*g*-PSA and 33DPP-*g*-PSA (again, all at 90–100% DOS) were loaded at varying DOX feed rates (Figure 6).

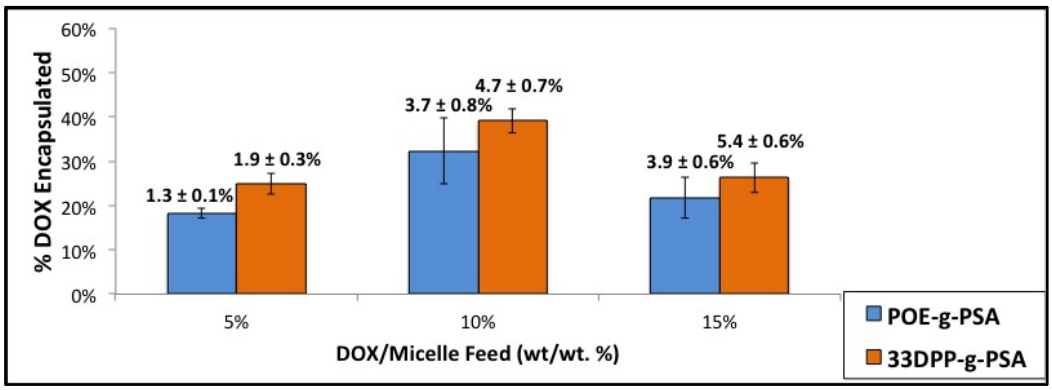

Figure 6. Micelle loading of selected PTAG-*g*-PSA reached an optimal level at a drug-to-polymer feed rate of 10%. Lower feed rates (5%) did not sufficiently load in enough DOX or stabilize the micelle. Higher feed rates (15%) stabilized the micelle, but may have resulted in DOX saturation and expulsion from the core. DOS of both PTAG-*g*-PSA formulations 90–100%. Loading capacity listed above error bars. P and D values within graphs designate post-hoc Tukey HSD test (see Supplemental materials).

Overall, 33DPP-*g*-PSA formulations had greater EE than their POE-*g*-PSA counterparts at each DOX feed rate. The longer, more hydrophobic chain of 33DPP-*g*-PSA resulted in more interaction sites between the drug and polymer chain and thereby higher loading potential. As the drug feed increased, the LC and EE of the micelles were sufficiently enhanced from 5 to 10%. While the micelles exhibited greater loading capacity at 15%, a noticeable drop-off was noted in their EE. Also of significant interest was the change in micelle size and PDI as DOX feed rate varied (Figure 7).

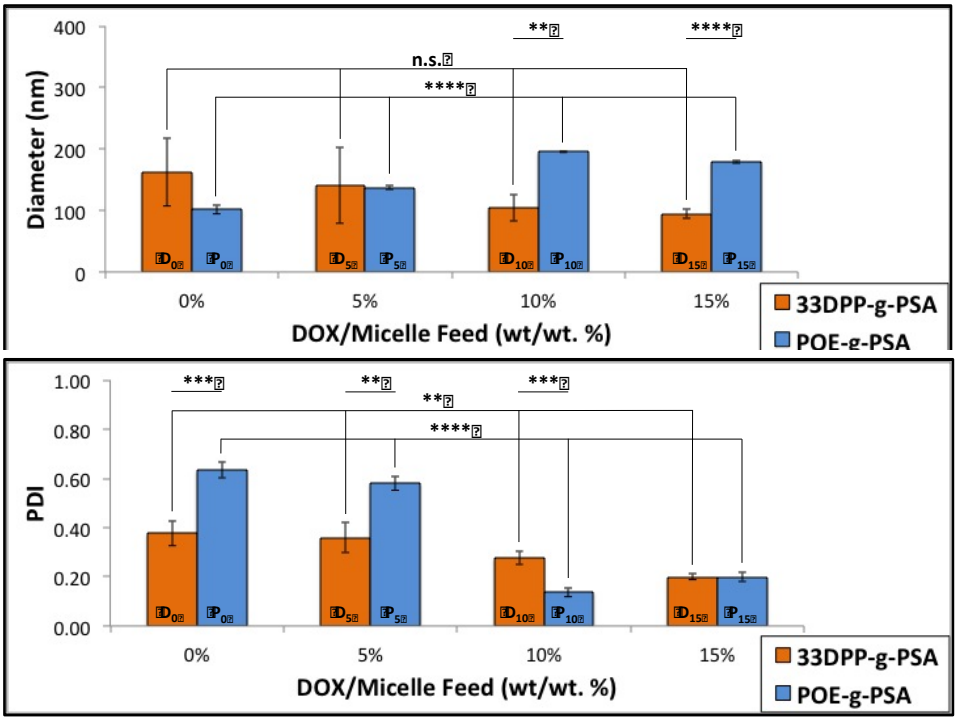

Figure 7. Micelles stabilize and form at different sizes based upon the composition of the core and the feed rate of DOX. 33DPP-*g*-PSA formulations already containing sufficient hydrophobicity formed smaller micelles at higher feed rates due to earlier micelle formation. POE-*g*-PSA micelles were more polar within their cores, potentially allowing for more DOX to be entrapped on a per micelle basis and leading to larger sizes upon DOX encapsulation based upon later micelle formation. The stabilizing of the micelle core is initiated only at a feed rate greater than 10% DOX. DOS of both PTAG-*g*-PSA formulations 90–100%. P and D values within graphs designate post-hoc Tukey HSD test (see Supplemental materials).

It can be readily seen that micelles, in general, decreased in dispersity and started to maintain stability with the introduction of as little as 5% DOX feed. Stability was enhanced with increasing DOX feed, noted by decreasing PDI proportional to increased DOX feed. Micelle size could also be greatly altered based upon the feed rate used. POE-*g*-PSA formulations increased in size while 33DPP-*g*-PSA decreased with increasing DOX respectively, indicating that a complete change in micelle self-assembly, and thereby size, can be made based upon the drug feed rate used. This confirms that 10% DOX feed was the optimal feed rate to maximize loading as well as form the most stable formulation based on the low PDI's obtained.

One of the problems most associated with micelles is their ability to remain stable upon dilution. Micelles are formed and kept together as a result of hydrophobic attractions between the core-forming chains. Their stability is strongly dependent on their concentration and upon dosage within the physiological environment will encounter a significant decrease in concentration. This can result in micelles falling apart and releasing their drug prematurely before reaching the target site. PTAG-*g*-PSA micelles were sufficiently increased in stability and size dispersion as a result of inclusion of DOX within the core (Figure 8).

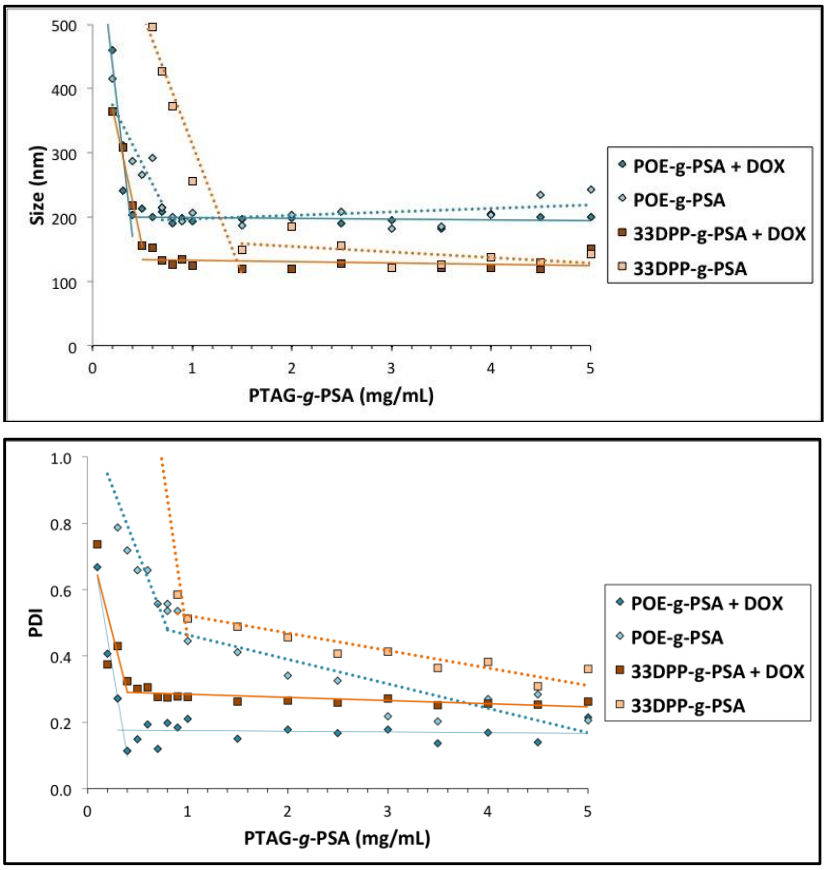

Figure 8. DOX loading within core results in significant micelle stabilization and resistance to dilution. Sizes (a) and PDI (b) were maintained at lower concentration values when loaded with DOX upon continual dilution at 37 ℃ in DD_2O, thereby indicating a drug-core stabilizing effect. This increased micelle stability makes drug-loaded micelles less prone to dilution when administered in circulation. DOS of both PTAG-*g*-PSA formulations 90–100%. Dotted and solid lines represent the average trend of unloaded and DOX-loaded micelles respectively.

Unloaded formulations of both POE-*g*-PSA and 33DPP-*g*-PSA both varied greatly in size and PDI upon continuous dilution. In contrast, drug loaded formulations of each respectively enhanced the PDI over their unloaded formulations and maintained relative monodispersity (PDI ~0.2) in size towards lower concentrations than unloaded counterparts. The PDI's of POE-*g*-PSA formulations were consistently less than 50% of 33DPP-*g*-PSA formulations. This can potentially be an indication of the attraction between the DOX and the select PTAG core group where lower, more stable PDI's at lower concentrations indicate a resistance to DOX leaving the core.

This correlation was further expanded when both micelles were assessed for release at pH 7.4 and 5.0 (Figure 9).

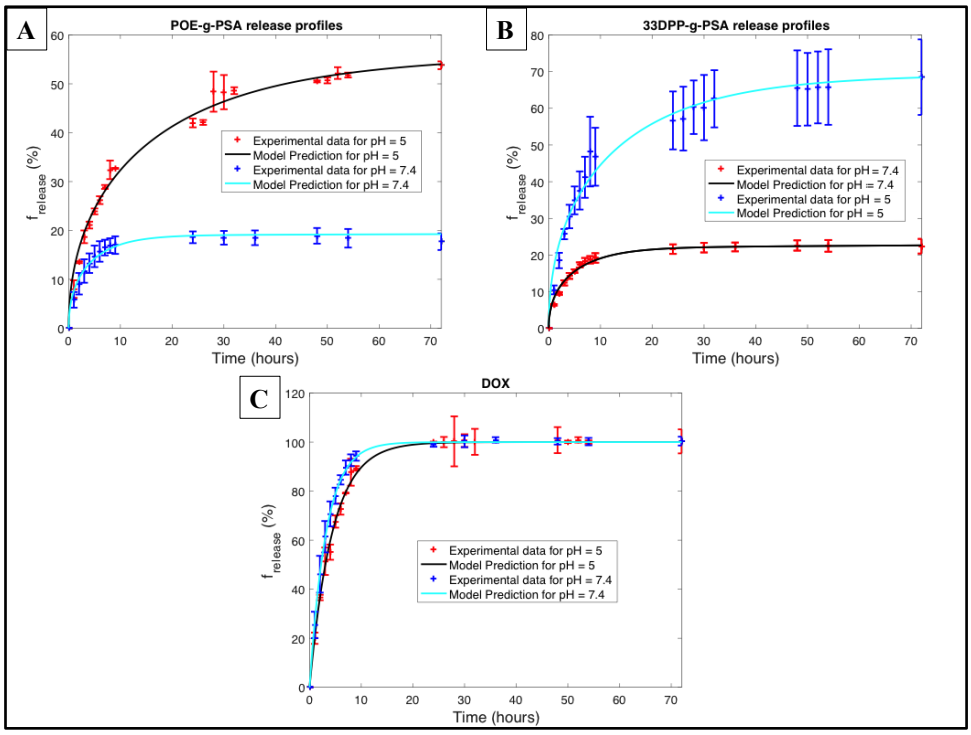

Figure 9. PSA micelles release DOX based upon internal composition and environmental pH. POE-*g*-PSA (a) containing a polar group release less DOX than 33DPP-*g*-PSA (b) containing an additional phenyl group at both lysosomal (pH 5.0) and physiological (pH 7.4). This indicates stronger bonding between drug and carrier in the non-polar micelle core of POE-*g*-PSA via hydrogen bonding than that added by hydrophobic attraction or π-π stacking by 33DPP-*g*-PSA. DOS of both PTAG-*g*-PSA formulations 90–100%. Free (unloaded) DOX (c) was used as a control. Release performed in phosphate buffer (pH 7.4, 37 ℃) or sodium acetate (pH 5.0, 37 ℃) at micelle equivalent of 350 μg/mL DOX.

These were selected to model micelle DOX release at both physiological (pH 7.4) and intracellular/lysosomal (pH 5.0) conditions. Nearly 100% of the free, unencapsulated DOX was released within 12 hours. At pH 7.4 both groups released a total of around 20% of the loaded DOX within the same 12-hour period, indicating that these micelles will remain stable at physiological circulation. This is comparable to other PSA formulations using short chain hydrophobic groups [44]. Interestingly, even at the same conditions and amount of DOX, POE-*g*-PSA (17.7 ± 1.7%) released less than 33DPP-*g*-PSA (22.5 ± 1.4%). This discrepancy was further widened between the two PTAG groups at pH 5.0 where the POE-*g*-PSA (53.8 ± 0.8%) released significantly less than 33DPP-*g*-PSA (70.5 ± 10.2%). This difference in drug release can be highly indicative of the potential bond strength between the PTAG group and the DOX. Root mean square errors (RMSE) of the fitting between the model prediction and experimental data for pH 5.0/7.4 were 1.7476%/0.799% for POE-*g*-PSA, 2.774%/0.727% for 33DPP-*g*-PSA and 2.727%/0.677% for free DOX.

The estimated values of φ_d^{burst}, k_d, $\overline{D}_d^*$ and t_d were calculated for POE-*g*-PSA, 33DPP-*g*-PSA and free DOX at both pH values assessed (Table 3).

Table 3. DOX release parameters of PSA micelles at pH 5.0 and pH 7.4. Quantification of the mass fraction of drug involved in the burst phase (φ_d^{burst}), the drug desorption rate constant (k_d), effective drug diffusivity ($\overline{D}_d^*$) and the drug induction time (t_d) in the drug release model shown in Eq 2 from drug release profiles for different particle types.

Type	pH	$\overline{D}_d^*$ ($cm^2\ s^{-1}$)	φ_d^{burst}	k_d (day^{-1})	t_d (hour)
POE-*g*-PSA	pH = 5.0	6.00×10^{-16}	4.7×10^{-1}	1.4×10^{-2}	4.17×10^{-2}
	pH = 7.4	2.21×10^{-15}	8.1×10^{-1}	1.0×10^{-3}	4.17×10^{-2}
33DPP-*g*-PSA	pH = 5.0	7.40×10^{-16}	3.2×10^{-1}	1.0×10^{-2}	4.17×10^{-2}
	pH = 7.4	1.84×10^{-15}	7.8×10^{-1}	2.7×10^{-3}	4.17×10^{-2}
DOX	pH = 5.0	NA	1	5.45	4.17×10^{-2}
	pH = 7.4	NA	1	7.46	4.17×10^{-2}

The model predictions were compared to the experimental release data, showing that the model can predict the experimental data with root mean square errors (RMSE) all less than 3%. Since DOX is the free drug without a diffusion phase through the PSA shell, φ_d^{burst} was set to 1 (i.e., 100% burst phase). For both POE-*g*-PSA and 33DPP-*g*-PSA, lowering pH decreased $\overline{D}_d^*$ and φ_d^{burst} but increased k_d. For DOX, lowering pH decreased k_d. φ_d^{burst} is lower in both POE-*g*-PSA and 33DPP-*g*-PSA when the drug DOX is embedded in these particles. Compared to 33DPP-*g*-PSA, POE-*g*-PSA offers a higher φ_d^{burst} and k_d but lower $\overline{D}_d^*$ for pH equal to 5.0. It is interesting to note that decreasing pH from 7.4 to 5.0 makes 33DPP-*g*-PSA have higher k_d but lower $\overline{D}_d^*$.

4. Discussion

Here, we have modified PSA with PTAG's (PTAG-*g*-PSA) of varying hydrophobic chain lengths (PEA, PPA, PBA), group polarity (POE) and number of phenyl groups (33DPP). Through this, we wished to explore how small changes in the hydrophobic component of these synthesized amphiphiles could ultimately result in large-scale effects (e.g., size, stability, loading/release). By using these specific PTAG groups, we aimed to understanding the effect that non-covalent intermolecular forces such as π-π stacking, hydrophobic attraction and hydrogen bonding could have on micelle drug loading and stability. Larger chained hydrophobic groups were not selected so as to isolate the effect of the small changes in the PTAG groups. Secondarily, longer chained groups tend to result in a double-edged sword effect between the high capacity to load yet the poor ability to release [50]. In tandem with understanding the variation in chain composition, we also wished to expand upon the rarely explored field of PSA micelle development for use in the delivery of cancer therapeutics. These studies aimed to provide the framework for future *in-vitro* work we are currently performing to use these micelles as potential intracellular drug delivery agents.

One of the most important aspects of any drug delivery carrier is to effectively control the size as well as size distribution (Poly Dispersity Index; PDI) [20]. Size, as previously noted, will dictate the ability for particles to avoid premature clearance by the RES, build up at a disease tissue site (e.g., the EPR effect for use within tumor targeting) and effectively be internalized by cells. Micelle size can be tailored based upon two specific, highly tailorable properties: Length of the hydrophobic chain and the extent at which the hydrophilic chain is substituted along its backbone by hydrophobic groups, the latter known as the degree of substitution (DOS). Micelle sizes are known to increase in size with increasing chain length of the hydrophobic group [12]. Deepagan et al. developed

amphiphilic Poly(caprolactone)-*b*-Poly(sialic acid) (PCL-*b*-PSA) via conjugation of PSA with various chain lengths of PCL (4k, 8k, 13k) [27]. These resulted in sizes of 270 ± 32 nm, 331 ± 75 nm and 390 ± 112 nm respectively for each increasing chain length assessed. Conversely, Zhang (Ursolic Acid-*g*-PSA, 120–150 nm) [44] and Bader [25] (DA-*g*-PSA, 25–150 nm) have both synthesized PSA micelles composed of short chain groups resulting in significantly smaller micelle sizes.

When alkyl chain length was increased sequentially in our PTAG-*g*-PSA formulations (PEA/PPA/PBA), the size of the micelle decreased, conflicting this idea. Potentially, due to the relative short lengths of all the evaluated PTAG chains, the micelles become significantly more compacted due to hydrophobic attraction. While lengthening of the alkyl chain may only be by one carbon, it significantly affects the percent hydrophobicity of the chain given the already small chain length. This results in smaller micelles with more hydrophobic/compact cores due to potential variations in self-assembly. Shorter chain lengths possess inherently less core hydrophobicity, thereby making it difficult in preventing water from entering the micelle core and increasing the hydrodynamic diameter [3]. Secondarily, micelle yields may be lower in shorter chain lengths due to difficulty in forming stable micelles, ultimately resulting in larger micelles from the fusion of smaller, less stable micelles or the increase in the critical agreggation number (CAC) needed for micelle formation [25]. This decreased core stability was exemplified in POE-*g*-PSA where the PTAG group expressed enhanced hydrophilicity from the addition of a polar oxygen to the chain. Sizes were larger for POE-*g*-PSA than other longer chained groups and greatly ranged in size. Similarly, these large fluctation of sizes can be perceived as a result of micelle instability from the difficulty in excluding water from the core, a mark of POE's hydrotropic nature, and potential micelle fusion. This was encountered in some synthesis, where the sizes reached nearly 300 nm (*data not shown*). Lastly, an additional phenyl moiety was assessed through the 33DPP-*g*-PSA formulation. This enhanced hydrophobicity was evident in the significant decrease in size compared to other groups. Micelles containing aromatic monomers have been shown to display smaller sizes as a result of more condensed cores, arising from π-π stacking and the hydrophobic effect exhibited between aromatic groups of adjacent polymer chains [17]. Further varying the number of hydrophobic groups aided towards enhancing the overall hydrophobicity of the amphiphile, such as was performed in 33DPP-*g*-PSA and POE-*g*-PSA formulations of varying DOS. This can further tailor micelle size by decreasing the CMC [25] and leading to smaller micelles [24].

The variation in micelle sizes confirmed here through simple core alterations yields many potential applications. The size of nanoparticles, as previously noted, used within nanomedicine applications will greatly dictate the residence time within circulation, immune system detection, premature clearance, passive tumor uptake, efficiency of intracellular uptake and ultimately the final intracellular destination. Due to the various sizes of DOX-loaded micelles obtained, these can ultimately be tailored for the targeting of specific sites within the body. Nanoparticles meant for long-circulating applications, tumor accumulation and cell uptake have been found to be most effective when between a specific size threshold. Particle circulation times can be drastically decreased if filtered out at certain sites within the body such as the kidney (<10 nm) [34], liver (<50 nm, >300 nm) [27] and RES (>200 nm) [27]. 200 nm has been viewed as the size cutoff which can take advantage of the EPR effect for use in passive tumor targeting [15], thereby making the ideal size between 70–200 nm [4] to avoid significant RES detection and filtration [12]. Micelles with wide size distributions will have difficulty in targeting the proper diseased site due to build up at different, non-targeted organs. The PDI of nanoparticle formulations is a parameter used to evaluate

the particle size distribution. Particles of all the same size (*monodisperse systems*) will exhibit low PDI's (<0.2) while systems of differing sizes (*polydisperse systems)* exhibit higher values, ranging anywhere from 0.3–0.5 for commonly seen micelles systems [10]. Relatively low PDI's and stable formulations have been noted by Zhao et al. as any micelle system ≤0.3 [48]. PDI's obtained in the assessed PTAG groups, while not as low as longer chain counterparts, are close to those found from other polysaccharide carriers bearing short chain alkyl groups, such as Stearate-*g*-Dextran [10] and Stearic Acid-*g*-Chitosan Oligosaccharide [6].

Once micelles are systemically administered they will immediately encounter a significant dilution, going from a highly concentrated to a significantly more dilute state. If diluted close to their CMC, micelles will form a larger size distribution from highly unstable ones falling apart and less stable formulations fusing together [34]. This phenomena was probably occuring in the cellular toxicity studies performed. When administered to cells, the unloaded, unstable micelles resulting from a relatively wide size distribution may have effectively fallen appart due or fused with more stable ones. This destabilization allowed for the interaction of the hydrophobic PTAG group and cell membrane, effectively inserting the PTAG group within the phospholipid bilayer once within sufficient proximity. Incorporation within the cell in situations like this allows for membrane fluidization and ultimately cellular toxocity. This has been noted in other studies where long alkyl chains, while beneficial for drug loading, were vastly harmful to cells [25]. This was seen in our studies, where increased DOS or hydrophobicity of the PTAG group greatly decreased biocompatability. Interestingly, the POE-*g*-PSA formulations were not toxic at any concentration tested. This may have been a result of the presence of the ether group decreasing the PTAG hydrophobicity and thereby its tendency to insert itself within the hydrophobic membrane layer.

Loading of DOX into the micelle had a drastic effect on micelle size and stability, essentially changing the point at which they reach their CMC. Hydrophobic drugs, when loaded into micelles, act as core-filling molecules and can enhance micelle stability substantially [20]. This can prevent micelles from falling apart once administered *in-vivo* and aid greatly towards in developing micelles with similar size distributions, thereby decreasing off-target side-effects resulting from RES filtration [20]. This enhanced micelle stability makes the interaction between the drug and the polymer essential. These interactions can be maximized by simple tailoring of the hydrophobic segment to match or exploit the properties of the loaded drug, in essence producing a "customized" carrier. This requires that a specific group or moiety of the hydrophobic chain (e.g., a phenyl group), be present so as to interact with a corresponding group (e.g., anthracene group) of the drug via a specific type of interaction (e.g., non-covalent π-π stacking). While effective, these types of interactions are mostly used in a synergistic effect in carriers so as to maximize loading. PBLG containing terminal phenyl groups as well as adjacent esters found in PBLG-*g*-Dextran micelles have been shown to aid in enhanced loading of DOX via π-π stacking and hydrogen bonding respectively [12]. Hydrophobic attraction and π-π stacking effects have also seen in linear-dendritic DOX-PEG drug-polymer conjugates, believed to be a result of π-π interactions between DOX anthracene rings stabilizing the core [5]. Due to the presence of the drug within the micelle, the hydrophobicity of the micelle core is sufficiently increased and the micelle is stabilized.

As compared to other micelles composed of long chain hydrophobic groups, there is significantly less area within the core binding sites for the drug to load within PTAG-*g*-PSA formulations, thereby greatly effecting the solubilization capacity of the micelle. This diminshed loading space can lead to "super-saturation" of the micelle core, intiating drug release into the

continuous phase and eventual crystallization/precipitation of the drug [18]. This may have been the case where drug feed was increased to 15% DOX in both POE-*g*-PSA and 33DPP-*g*-PSA formulations. As the DOX content increases, there is also an indication that DOX may physically aggregate together as a result of chemically bonding with itself and forming a dimer [50]. As a result, more careful consideration should be taken when selecting the amount of drug to load within the micelle as, in this case, less is more.

Larger core size has been suggested to have positive influence on the ability for the carrier to solubilize the drug [18]. While loading may be increased with longer chain lengths [12,13], a saturation point is ultimately reached due to enhanced crystallinity of the longer chain, a negative for drug loading [24]. For example, Hyaluronic acid-*g*-$PLGA_{5\text{-}10k}$ micelles composed of a much longer hydrophobic segment (5–10 kDa) exhibited a LC of 4.8–7.2 wt.% DOX and EE of 20.2–31.0 wt.% [49], both of which were met or exceeded using the simple short chain PTAG variations presented here. This may potentially mean that the composition of the chain, and not necessarily the length, is the most important factor when designing micelles. While less than than covalent or ionic bonds (500 kJ/mol), a synergistic approach combining Hydrogen bonding (10–40 kJ/mol), π-π stacking (8–9 kJ/mol), van der Waal forces (1 kJ/mol) and entropic/hydrophobic interactions may be potent enough to enhance drug loading [3]. The loading of the drug within the micelle can only take place on a limited amount of sites if the core is composed of groups of sufficiently small chain length. In the case of these PTAG-*g*-PSA micelles, we believe that the DOX is loaded via a potential synergistic effect between its attraction to the PTAG chain ("free chain") as well as other loaded DOX molecules which have already interacted with the chain ("saturated chain"). This can allow for DOX to load in upon itself via sequential π-π stacking to the saturated chain, thereby allowing for more drug to be loaded. This DOX-DOX π-π stacking has been noted previously with linear-dendritic DOX-PEG drug-polymer conjugates [5].

Secondarily, this PTAG/DOX_1-DOX_2—DOX_n stacking can be seen as a collective cohesive effect where DOX molecules may potentially "sandwich" together. The PTAG chains can act as initiator or stabilizer sites where the sequential π-π stacking can start as a result of enhanced hydrophobicity stemming from the formation of PTAG/DOX_1-DOX_2—DOX_n "sandwich" chains. This DOX "sandwiching" continues, effectively stabilizing the micelle core from other PTAG/DOX_1-DOX_2—DOX_n sandwich chains arising from other PTAG-*g*-PSA amphiphiles. Ultimately, a condensed micelle core of multiple PTAG/DOX_1-DOX_2—DOX_n chains can be formed, resulting in the DOX stabilized micelles seen in both the size and PDI measurements. Yet, as a result of these lack of "binding" or "initiating" sites due to the short chain length, DOX which is already stabilized within the micelle may diffuse out or interact with other free DOX not associated with the micelle core, effectively limiting the amount of DOX which can be loaded inside. Problems arise when the micelle reaches this point of micelle core super-saturation where the drug will begin to precipitate out and no longer be encapsulated. This, again, makes the selection of the correct feed rate of drug essential towards maximizing drug loading and carrier stabilization. Any more excess drug added may exceed the core capacity of these micelles to load. Excess free drug can then potentially form large agreggates and act as a drug leaching or sequestering agent, agreggating with drug that could have been inside the core but instead interacted with these free drug aggregates.

In the same vein, *intra*- or *inter*-polymer interactions within the PTAG core may have excluded DOX and limited loading potential. Pendent phenyl groups from either the same PTAG-*g*-PSA amphiphile ("*intra*") or other PTAG-*g*-PSA amphiphiles ("*inter*") may have preferentially interacted

within one another rather than the drug. That is why selecting a type of interaction to be exclusive between drug and carrier would be preferential so as to eliminate this potential competitive inhibition. The ability to maximize drug loading may simply come down to designing a micelle core that would match the properties of the drug. This match would entail selecting a group that would enhance interactions with the drug and maximize loading. The discrepancy between the composition of POE-*g*-PSA and 33DPP-*g*-PSA in hydrophobicity is significant, with POE-*g*-PSA even containing polar elements which can hinder micelle formation, yet these both loaded almost the same amount of DOX. This can be attributed to both the strength of additional hydrogen bonding (10–40 kJ/mol) over additional π-π stacking (8–9 kJ/mol)/hydrophobicity, the strength of hydrogen bonding within a non-polar environment and the interaction probability. There are more hydrogen bonding donors and acceptors than π-π stacking sites (anthracene rings) on DOX, thereby making the addition of a hydrogen bond acceptor/ether of POE-*g*-PSA more valuable than the addition of alkyl and phenyl groups of 33DPP-*g*-PSA. Therefore when tailoring a delivery vehicle towards exploiting a specific drug/carrier interaction (e.g., π-π stacking), there should be sufficient sites on both the drug and carrier for sufficient exploitation.

Release studies also indicated a trend towards stronger interactions between POE/DOX than 33DPP/DOX. This strongly implies that the specific non-covalent attraction between DOX and the selected PTAG group will dictate how the drug will be released once in circulation. Hydrogen bonding is known to be stronger than π-π stacking and, as stated previously, is stronger in non-polar environments such as the micelle core than in polar environments where water can interfere. This would explain the reason for less DOX being released from the POE-*g*-PSA micelles as compared to the 33DPP-*g*-PSA formulations. The small discrepancy between the two at pH 7.4 was enhanced to an even greater extent at pH 5.0. The solubility of DOX is strongly dependent upon pH where the solubility can increase nearly 6 fold from 0.0625 mg/mL at pH 7.4 to 0.37 mg/mL at pH 5.0 [50]. As the solubility of the DOX in the buffer increases, the drug partition coefficient in the polymeric media will decrease and result in enhanced drug release into the buffer [50]. DOX release has been shown to be faster and nearly 50% greater at pH 5.0 than 7.4 in release studies performed with PLA-*b*-PEG micelles [50]. These results were comparable to our formulations.

Release of drugs from the polymer matrix is governed by a combination of pure diffusion and erosion control, that of which are effected by a significant number of processes. These include polymer composition, molecular weight, hydrophilicity, crystallinity, micelle size, porosity, surface character, possible swelling of the matrix, polymer erosion or degradation, dissolution of the drug and internal/external mass transport of the dissolved drug [50,52]. The drug release from micelles occurs in two phases—a burst, or induction, phase, and a diffusion phase. The induction phase consists of an initial burst of drug release due to desportion from mesopores and from the outer surface of the particle. The diffusion phase involves diffusion of the drug out of the PSA shell as the shell degrades through pores forming during hydration, degradation, and erosion of particles. Parameters φ_d^{burst}, k_d, $\bar{D}_d^*$ and t_d play an important role in regulating the release profiles. In particular, φ_d^{burst} regulates the final value of $f_{release}$; k_d influences the slopes of the release profiles over time; $\bar{D}_d^*$ changes the curvature of $f_{release}$. These were estimated via a nonlinear least square approach to minimize the difference between the model prediction of f_{release} and the experimental release profiles.

Yet the most important part of drug release may lie in the basic drug/core interactions for polymer micelles in the field of cancer therapy [53,54]. In comparison of the release of DOX

PCL-*b*-PEG and PLA-*b*-PEG, it was found that the group which interacted the most with DOX (PCL; 5-6 hydrogen bonds with DOX) released significantly more than the group which interacted the least (PLA; 3-4 hydrogen bonds with DOX) [50]. This leads to less attractive force between the DOX and PLA and thereby the reason for its larger release. In the case of 33DPP-*g*-PSA, which only had one area for hydrogen bonding (carbonyl), the release was less than POE-*g*-PSA which had another (ether). This indicates it is not just the length but the composition of the internal chain that matters.

5. Conclusion

Here we have modified poly (sialic acid) (PSA) with short chain phenyl-terminated alkyl groups (PTAGs) to form PTAG-*g*-PSA which self-assemble under aqueous conditions to form micelles. PTAG variations included changes in group hydrophobicity (alkyl chain addition), polarity (internal core hydrogen bonding sites) and π-π stacking sites to exploit non-covalent interactions between the chemotherapeutic DOX and the respective PTAG group. These small alterations resulted in large characterization changes of the micelles such as size, stability, cellular toxicity, loading and release. The relative instability of unloaded formulations was stabilized through the addition of DOX upon drug loading. The % DOX loaded proved to be a crucial parameter in the amount of drug which could be loaded as either too little (insufficient payload/micelle stability) or too much (drug crystallization and precipitation) proved detrimental towards the loading and stability of the micelle. Drug loading was relatively similar in PTAG chains which benefited from additional hydrogen bonding (POE-*g*-PSA) or π-π stacking (33DPP-*g*-PSA), indicating that similar loading can be accomplished based upon differing drug/chain interactions. DOX release from POE-*g*-PSA was significantly inhibited compared to 33DPP-*g*-PSA as a result of stronger drug/chain hydrogen bonding interactions in comparison to additional π-π stacking. Based upon these results, we believe that the interactions between the drug and core-forming segment should be an essential design parameter. By doing this, a new generation of "custom-designed" carriers can maximize the potential of nanoparticles as therapeutic delivery platforms.

Secondarily, the hydrophilic coating should be of the same utmost importance given its significance in protecting the carrier from premature clearance and providing a relative means of controlled carrier targeting. Given their characteristics, we are currently investing these PTAG-*g*-PSA micelles as potential intracellular delivery agents for the treatment of various types cancer.

Equations

$$\text{Loading Capacity} = \frac{M_{DOX-Encapsulated}}{M_{Micelles-Feed}} \times 100\% \quad (1)$$

Where $M_{Dox\text{-}Encapsulated}$ is the weight of DOX in the micelles and $M_{Micelles\text{-}Feed}$ is the weight of DOX-loaded micelles.

$$\text{Encapsulation Efficiency} = \frac{M_{DOX-Encapsulated}}{M_{DOX-Feed}} \times 100\% \quad (2)$$

Where $M_{Dox\text{-}Encapsulated}$ is the weight of DOX in the micelles and $M_{DOX\text{-}Feed}$ is the weight of DOX in the feed.

$$f_{release} = \varphi_d^{burst}(1-e^{-k_d t}) + (1-\varphi_d^{burst})(1-\frac{6}{\pi^2}\sum_{j=1}^{\infty}\frac{-e^{-j^2\pi^2\overline{D}_d^*(t-t_d)/r_0^2}}{j^2}) \quad (3)$$

Where $f_{release}$ is the model-predicted mass fraction of released drug, φ_d^{burst} is the mass fraction of drug involved in the burst phase, k_d is the drug desorption rate constant, $\overline{D}_d^*$ is the effective drug diffusivity, t_d is the drug induction time (i.e., the time for micropores to form), and r_0 is the initial micelle radius.

Acknowledgments

This research was funded from an internal endowment grant from Villanova University.

Conflict of interest

The authors of this paper declare no conflicts of interest in this paper.

References

1. Caliceti P, Salmaso S (2013) Stealth properties to improve therapeutic efficacy of drug nanocarriers. *J Drug Deli* 2013: 1–19.
2. Jayant S, Khandare JJ, Wang Y, et al. (2007) Targeted sialic acid-doxorubicin prodrugs for intracellular delivery and cancer treatment. *Pharm Res* 24: 2120–2130.
3. Li Y, Yang L (2015) Driving forces for drug loading in drug carriers. *J Microencapsu* 32: 255–272.
4. Wang XH, Tian Q, Wang W, et al. (2012) In vitro evaluation of polymeric micelles based on hydrophobically-modified sulfated chitosan as a carrier of doxorubicin. *J Mater Sci-Mater M* 23: 1663–1674.
5. Li JF, Yang HY, Zhang YJ, et al. (2015) Choline Derivate-Modified Doxorubicin Loaded Micelle for Glioma Therapy. *Acs Appl Mater Inter* 7: 21589–21601.
6. Su Y, Hu Y, Du Y, et al. (2015) Redox-responsive polymer drug conjugates based on doxorubicin and chitosan oligosaccharide-g-stearic acid for cancer therapy. *Mol Pharm* 12: 1193–1202.
7. Gou P, Liu W, Mao W, et al. (2013) Self-assembling doxorubicin prodrug forming nanoparticles for cancer chemotherapy: Synthesis and anticancer study in vitro and in vivo. *J Mater Chem B* 1: 284–292.
8. Sun Y, Zou W, Bian SQ, et al. (2013) Bioreducible PAA-g-PEG graft micelles with high doxorubicin loading for targeted antitumor effect against mouse breast carcinoma. *Biomaterials* 34: 6818–6828.
9. Jain RK, Stylianopoulos T (2010) Delivering nanomedicine to solid tumors. *Nat Rev Clin Oncol* 7: 653–664.
10. Du YZ, Weng Q, Yuan H, et al. (2010) Synthesis and antitumor activity of stearate-g-dextran micelles for intracellular doxorubicin delivery. *Acs Nano* 4: 6894–6902.

11. Wang YC, Wang F, Sun TM, et al. (2011) Redox-responsive nanoparticles from the single disulfide bond-bridged block copolymer as drug carriers for overcoming multidrug resistance in cancer cells. *Bioconjugate Chem* 22: 1939–1945.
12. Zhang AP, Zhang Z, Shi FH, et al. (2013) Redox-sensitive shell-crosslinked polypeptide-block-polysaccharide micelles for efficient intracellular anticancer drug delivery. *Macromol Biosci* 13: 1249–1258.
13. Shuai XT, Ai H, Nasongkla N, et al. (2004) Micellar carriers based on block copolymers of poly(e-caprolactone) and poly(ethylene glycol) for doxorubicin delivery. *J Control Release* 98: 415–426.
14. Song HT, Hoang NH, Yun JM, et al. (2016) Development of a new tri-block copolymer with a functional end and its feasibility for treatment of metastatic breast cancer. *Colloids Surface B* 144: 73–80.
15. Zhao XY, Poon Z, Engler AC, et al. (2012) Enhanced stability of polymeric micelles based on postfunctionalized poly(ethylene glycol)-b-poly(gamma-propargyl L-glutamate): The substituent effect. *Biomacromolecules* 13: 1315–1322.
16. Hamaguchi T, Matsumura Y, Suzuki M, et al. (2005) NK105, a paclitaxel-incorporating micellar nanoparticle formulation, can extend in vivo antitumour activity and reduce the neurotoxicity of paclitaxel. *Brit J Cancer* 92: 1240–1246.
17. Shi Y, van Steenbergen MJ, Teunissen EA, et al. (2013) Pi-Pi stacking increases the stability and loading capacity of thermosensitive polymeric micelles for chemotherapeutic drugs. *Biomacromolecules* 14: 1826–1837.
18. Carstens MG, de Jong P, van Nostrum CF, et al. (2008) The effect of core composition in biodegradable oligomeric micelles as taxane formulations. *Eur J Pharm Biopharm* 68: 596–606.
19. Yokoyama M, Fukushima S, Uehara R, et al. (1998) Characterization of physical entrapment and chemical conjugation of adriamycin in polymeric micelles and their design for in vivo delivery to a solid tumor. *J Control Release* 50: 79–92.
20. Kataoka K, Matsumoto T, Yokoyama M, et al. (2000) Doxorubicin-loaded poly(ethylene glycol)-poly(beta-benzyl-l-aspartate) copolymer micelles: Their pharmaceutical characteristics and biological significance. *J Control Release* 64: 143–153.
21. Hofman JW, Carstens MG, van Zeeland F, et al. (2008) Photocytotoxicity of mTHPC (temoporfin) loaded polymeric micelles mediated by lipase catalyzed degradation. *Pharm Res* 25: 2065–2073.
22. Mikhail AS, Allen C (2010) Poly(ethylene glycol)-b-poly(epsilon-caprolactone) micelles containing chemically conjugated and physically entrapped docetaxel: Synthesis, characterization, and the influence of the drug on micelle morphology. *Biomacromolecules* 11: 1273–1280.
23. Wang C, Chen B, Zou M, et al. (2014) Cyclic RGD-modified chitosan/graphene oxide polymers for drug delivery and cellular imaging. *Colloid Surface B* 122: 332–340.
24. Yan JL, Ye ZY, Chen M, et al. (2011) Fine tuning micellar core-forming block of poly(ethylene glycol)-block-poly(epsilon-caprolactone) amphiphilic copolymers based on chemical modification for the solubilization and delivery of doxorubicin. *Biomacromolecules* 12: 2562–2572.
25. Bader RA, Silvers AL, Zhang N (2011) Polysialic acid-based micelles for encapsulation of hydrophobic drugs. *Biomacromolecules* 12: 314–320.

26. Veronese FM, Pasut G (2005) PEGylation, successful approach to drug delivery. *Drug Discov Today* 10: 1451–1458.
27. Deepagan VG, Thambi T, Ko H, et al. (2013) Amphiphilic polysialic acid derivatives: Synthesis, characterization, and in-vitro cytotoxicity. *J Nanosci Nanotechno* 13: 7312–7318.
28. Gregoriadis G, McCormack B, Wang Z, et al. (1993) Polysialic acids—potential in drug delivery. *Febs Lett* 315: 271–276.
29. Konradi R, Acikgoz C, Textor M (2012) Polyoxazolines for nonfouling surface coatings—a direct comparison to the gold standard PEG. *Macromol Rapid Comm* 33: 1663–1676.
30. Bondioli L, Ruozi B, Belletti D, et al. (2011) Sialic acid as a potential approach for the protection and targeting of nanocarriers. *Expert Opin Drug Del* 8: 921–937.
31. Semple SC, Harasym TO, Clow KA, et al. (2005) Immunogenicity and rapid blood clearance of liposomes containing polyethylene glycol-lipid conjugates and nucleic acid. *J Pharmacol Exp Ther* 312: 1020–1026.
32. Amoozgar Z, Yeo Y (2012) Recent advances in stealth coating of nanoparticle drug delivery systems. *Wires Nanomed Nanobio* 4: 219–233.
33. Zhang N, Wardwell PR, Bader RA (2013) Polysaccharide-based micelles for drug delivery. *Pharmaceutics* 5: 329–352.
34. Wilson DR, Zhang N, Silvers AL, et al. (2014) Synthesis and evaluation of cyclosporine A-loaded polysialic acid-polycaprolactone micelles for rheumatoid arthritis. *Eur J Pharm Sci* 51: 146–156.
35. Bondioli L, Costantino L, Ballestrazzi A, et al. (2010) PLGA nanoparticles surface decorated with the sialic acid, N-acetylneuraminic acid. *Biomaterials* 31: 3395–3403.
36. Deninno MP (1991) The synthesis and glycosidation of n-acetylneuraminic acid. *Synthesis* 1991: 583–593.
37. Rutishauser U (1998) Polysialic acid at the cell surface: Biophysics in service of cell interactions and tissue plasticity. *J Cell Biochem* 70: 304–312.
38. Vodovozova EL, Moiseeva EV, Grechko GK, et al. (2000) Antitumour activity of cytotoxic liposomes equipped with selectin ligand SiaLe(X), in a mouse mammary adenocarcinoma model. *Eur J Cancer* 36: 942–949.
39. Hirai M, Minematsu H, Hiramatsu Y, et al. (2010) Novel and simple loading procedure of cisplatin into liposomes and targeting tumor endothelial cells. *Int J Pharm* 391: 274–283.
40. Zheng JS, Zheng SY, Zhang YB, et al. (2011) Sialic acid surface decoration enhances cellular uptake and apoptosis-inducing activity of selenium nanoparticles. *Colloid Surface B* 83: 183–187.
41. Greco F, Arif I, Botting R, et al. (2013) Polysialic acid as a drug carrier: evaluation of a new polysialic acid-epirubicin conjugate and its comparison against established drug carriers. *Polym Chem-UK* 4: 1600–1609.
42. Zeisig R, Stahn R, Wenzel K, et al. (2004) Effect of sialyl Lewis X-glycoliposomes on the inhibition of E-selectin-mediated tumour cell adhesion in vitro. *Biochim Biophys Acta* 1660: 31–40.
43. Gajbhiye V, Ganesh N, Barve J, et al. (2013) Synthesis, characterization and targeting potential of zidovudine loaded sialic acid conjugated-mannosylated poly(propyleneimine) dendrimers. *Eur J Pharm Sci* 48: 668–679.

44. Zhang WX, Dong DQ, Li P, et al. (2016) Novel pH-sensitive polysialic acid based polymeric micelles for triggered intracellular release of hydrophobic drug. *Carbohyd Polym* 139: 75–81.
45. Ray GB, Chakraborty I, Moulik SP (2006) Pyrene absorption can be a convenient method for probing critical micellar concentration (cmc) and indexing micellar polarity. *J Colloid Interf Sci* 294: 248–254.
46. Hans M, Shimoni K, Danino D, et al. (2005) Synthesis and characterization of mPEG-PLA prodrug micelles. *Biomacromolecules* 6: 2708–2717.
47. Liang HC, Chang WH, Liang HF, et al. (2004) Crosslinking structures of gelatin hydrogels crosslinked with genipin or a water-soluble carbodiimide. *J Appl Polym Sci* 91: 4017–4026.
48. Koo AN, Min KH, Lee HJ, et al. (2012) Tumor accumulation and antitumor efficacy of docetaxel-loaded core-shell-corona micelles with shell-specific redox-responsive cross-links. *Biomaterials* 33: 1489–1499.
49. Lee H, Ahn CH, Park TG (2009) Poly lactic-co-(glycolic acid)-grafted hyaluronic acid copolymer micelle nanoparticles for target-specific delivery of doxorubicin. *Macromol Biosci* 9: 336–342.
50. Sutton D, Wang S, Nasongkia N, et al. (2007) Doxorubicin and beta-lapachone release and interaction with micellar core materials: experiment and modeling. *Exp Biol Med* 232: 1090–1099.
51. Donaldson O, Huang Z, Comolli N (2013) An integrated experimental and modeling approach to propose biotinylated PLGA microparticles as versatile targeting vehicles for drug delivery. *Prog Biomat* 2: 1–10.
52. Zhai S, Ma Y, Chen Y, et al. (2014) Synthesis of an amphiphilic block copolymer containing zwitterionic sulfobetaine as a novel pH-sensitive drug carrier. *Polym Chem* 5: 1285–1297.
53. Deshmukh AS, Chauhan PN, Malleshappa NN, et al. (2017) Polymeric micelles: Basic research to clinical practice. *Int J Pharm* 532: 249–268.
54. Aftab S, Shah A, Nadhman A, et al. (2018) Nanomedicine: An effective tool in cancer therapy. *Int J Pharm* 540: 132–149.

AIMS Press